Near-Strain-Free GaN/AlGaN Narrow Line Width UV Light Emission with Very Stable Wavelength on Excitation Power by Using Superlattices

Mo Li, Feiliang Chen, Claudius Kocher, Hui Zhang, Shuxiao Li, Feng Huang, Jian Zhang, and Robert A. Taylor

Abstract

Because of the strong strain in nitrides, superlattice layers have been used to release the strain in the QW and reduce the quantum confined Stark effect. However, few reports discuss comprehensively the strain relaxation behavior and optical performance of a GaN/AlGaN single quantum well (QW) with inserted GaN/AlGaN superlattices (SLs). In this work, we examined a group of graded Al content GaN/ $Al_xGa_{1-x}N$ SL layers under the GaN/$Al_{0.3}Ga_{0.7}N$ single QW grown on c-plane sapphire. Both the excitation power and temperature dependence of the time-integrated microphotoluminescence (μ-PL) and time-resolved μ-PL were measured. The samples exhibited very narrow UV emission and had almost unchanged emission wavelength and stable line width behavior with excitation power as well as "S-shape" and weak "W-shape" characteristics with temperature due to the localization. The temperature-dependent PL lifetime was measured from 5 to 300 K, and the relatively fast recombination lifetime of the two samples was examined. Micro-Raman spectroscopy was also conducted to probe the strain state. All the results showed that adopting SLs around the QW structure produced a much more stable and desirable performance, which can be attributed to an effective relaxation of the strain in the QW.

Introduction

GaN/AlGaN quantum wells (QWs) grown on sapphire substrates have attracted considerable attention as promising candidates for ultraviolet (UV) light sources, including light emitting
diodes and laser diodes,[1,2] with a wide range of applications in medicine, biochemistry, sensing, and communications. [3,4] Although a good deal of progress has been achieved, the growth of high-quality GaN/AlGaN heterostructures is still challenging. Different thermal expansion coefficients and a large lattice mismatch between nitride materials and substrates introduce a high density of defects (threading dislocations, cracks, etc.), inevitable built-in strain, and strong spontaneous and piezoelectric polarization. As a result, the strain-induced quantum confined Stark effect (QCSE) results in spatial separation of electrons and holes within tilted potential wells.[5,6] This leads to a red-shift of the emission wavelength and a reduction of recombination rate, which adversely affects the stability and reliability of fabricated devices. A high Al content will aggravate the above problems. Different schemes have been applied to overcome the difficulties; one scheme is to grow the nonpolar QW, which is free of polarization-induced strain with significantly improved crystal quality.[7,8] Another commonly used method is to insert strain engineering layers under the QWs, among which In(Ga)N/GaN superlattices (SLs) have been widely reported and proved to be efficient on releasing the strain, thereby avoiding the formation of cracks and improving the device's characteristics.[9−11] The use of GaN/Al(Ga)N SLs as the strain relaxing layer was also investigated, and the quality and strain status of the nitride films and heterostructures deposited on them were determined, but these studies mainly focused on the growing

conditions by using different epitaxial methods.[12−16] Very few reports have been published discussing in depth how the SLs as strain relaxation layers affect and contribute to the improved optical performance of the GaN/ AlGaN QW emission. Detailed analyses of the emission wavelength, line width, and recombination dynamics of GaN/ AlGaN QW with strain-relaxing SLs are still lacking.

In this paper, we propose a GaN/$Al_{0.3}Ga_{0.7}N$ single QW grown on a c-plane sapphire substrate with embedded GaN/AlGaN SLs. To examine the strain-relaxing effects of the SLs, a nanopillar sample fabricated by a top-down method is used for comparison with the parent as-grown sample. Time-integrated micro-photoluminescence (TI-μPL), time-resolved μ-PL (TR-μPL), and micro-Raman (μ-Raman) spectroscopy experiments are conducted to investigate the strain state and the optical performance of the two samples. We find that the strain of the two samples is almost fully released, which is generally observed in nonpolar structures. The QW emission in the UV region is very narrow even at room temperature. Moreover, they have a nearly constant QW emission wavelength and only a small line width broadening with increasing excitation power. The two samples also have a relatively fast radiative recombination time at 5 K. The physical mechanisms underlying these properties were discussed. All the results confirm that the QW structure with embedded SL layers has improved performance, paving the way to stable optoelectronic UV devices.

Experiments

The planar as-grown sample was epitaxially grown in the following steps: First, a 25 nm thick AlN layer was grown on a (0001) c-plane oriented pyramidal array patterned sapphire substrate (PSS) by using an Aixtron CRIUS I vertical close-spaced metal−organic chemical vapor deposition reactor at 500°C, followed by a 2300 nm thick $Al_{0.1}Ga_{0.9}N$ layer grown at 1250°C. Second, the two groups GaN/$Al_{0.15}Ga_{0.85}N$ (3 periods) and GaN/$Al_{0.2}Ga_{0.8}N$ SLs (9 periods) were grown at 1250°C. The thickness of the GaN layer was about 8 nm, and that of the $Al_xGa_{1-x}N$ layer was about 2 nm. Then two 200 nm undoped Al0.3Ga0.7N barrier layers and 1 nm GaN well layer were grown at 1250°C for 2100 and 100 s, respectively. Figure 1 shows the schematic structure of the planar sample. An important part of the design is the increasing Al mole fraction of the structure from bottom to top to match the thermal expansion coefficients and lattice constants between the substrate and the QW, including the $Al_{0.1}Ga_{0.9}N$ layer and SLs. Figures 2a and 2b show the TEM images of the single QW and the SLs in different scales. The interfaces between the QW and the barriers can be observed clearly. It only shows some moderate fluctuations of the width of the well, which leads to the localized states. From Figure 2b and TEM images in larger scales (not presented here), the growth quality of the SLs is good; no obvious bending, dislocations, or inhomogeneities of the periodic structures are visible, which to a certain extent proves that the strain in the SLs is relaxed and contributes to the quality of the QW.

After the epitaxial growth, nanopillars were fabricated by self-assembled polystyrene (PS) microsphere lift-off lithography. The monolayer of the PS microsphere was transferred on the top of the as-grown sample, and then gold was deposited by electron beam evaporation, filling the gaps between the microspheres. After the microspheres were removed, the remaining gold pattern was used as a mask for the inductively coupled plasma (ICP) etching to obtain nanocones. This process produced surface damage and roughness together with angled sidewalls for the nanocones. Hence, a wet etching process with KOH solution was applied to yield narrower nanopillars with vertical sidewalls and also to remove the surface defects. A large number of nanopillars with an average diameter of <70 nm and a height of ~300 nm are shown in Figure 2c. Size fluctuation of the nanopillars is caused by the inhomogeneous alignment and the varying diameters of the PS microspheres.

For all the μ-PL measurements, the samples were held in a continuous flow Janis ST-500 cryostat equipped with a heater (with a feedback loop) so that the range of accessible temperatures was 4.2−300 K, with a temperature stability of about 50 mK. The frequency-tripled output (λ = 266 nm) of a Ti:Al_2O_3 pulsed laser with 100 fs pulse width and 80 MHz repetition rate was used as the excitation source. The laser was focused on the sample by a 40× UV objective with a numerical aperture (NA) of 0.4. The excited PL was collected by the same objective, dispersed by a 0.3 m long spectrometer with a 600 lines/mm grating, and detected by a thermoelectrically cooled charge-coupled device (CCD). For the TR-μPL, a photomultiplier tube (PMT) with about 130 ps response time and a time-correlated single-photon-counting (TCSPC) card with a bin width of 25 ps were used. Micro-Raman backscattering spectroscopy was performed at room temperature by using an intracavity doubled Nd^{3+}:YAG laser with a linear polarized output and a wavelength of 532 nm. The polarization direction of the incident light was controlled by a halfwave plate before the objective, and the polarization of Raman signal was selected by a polarizer in front of the spectrometer. The Raman spectra were detected by using the same CCD and spectrometer but using a 1200 lines/mm grating.

Results and Discussion

Figure 3 shows the TI-μPL spectra of the two samples measured at 5 and 300 K with 5 μW excitation power. Each PL spectrum was taken five times and then averaged to account for any laser power fluctuations. Gaussian fitting was used to obtain the peak positions and the full width at half-maximum (fwhm). At 5 K, the peaks at about 327, 346, and 348 nm are from the QW, GaN/$Al_{0.2}Ga_{0.8}N$ SL layer, and GaN/$Al_{0.15}Ga_{0.85}N$ SL layer, respectively; the peaks at about 356 and 357 nm are the emissions from the Al0.1Ga0.9N buffer layer and the GaN layers, respectively. The QW line widths of the as-grown sample and the nanopillar sample are very narrow, which are 16.8 ± 0.4 meV (1.47 nm) and 18.6 ± 0.2 meV (1.63 nm), respectively, indicating good growth quality and quantum confinement. After passing through the silica window of the cryostat, the spot size of the laser is about 2 μm and covers several nanopillars. This makes the PL spectra of the nanopillars a little bit wider than that of the as-grown sample, arising from pillar-to-pillar size fluctuation and quantum confinement dispersion. Carrier-to-carrier interactions, surface trapping, or scattering may also contribute to the PL broadening at higher temperatures. According to published reports on nitride polar-plane nanopillars, the QW peak wavelength of nanopillar samples shows obvious blue-shifts compared to that of the parent as-grown samples due to the reduced QCSE in the wells.[17,18] For our samples, the QW wavelengths depend on the excited position of the samples.

They vary from about 327.4 to 328.7 nm for as-grown sample and from about 326.6 to 327.8 nm for nanopillars at 5 K (the inset of Figure 3a shows the position-dependent PL spectra of the as-grown sample at 5 K). This variation arises due to thickness fluctuations of the QW as well as Al composition inhomogeneity in the barriers and SLs, which influence the confinement and strain states of the layers and further change their emission energies. It is worth noting that the peaks around 356 and 357 nm are almost position independent, proving that the two peaks are from the 2300 nm thick $Al_{0.1}Ga_{0.9}N$ layer and the GaN in the SLs, which are not strongly affected by strain and nonuniform composition. In spite of the peak fluctuations, the wavelength variation range of the nanopillars exhibits a small blue-shift compared to that of the as-grown samples of about 0.8−0.9 nm, as strain relaxation reduces the QCSE. When the temperature is increased to 300 K, all the peaks shift to longer wavelengths and become broader. The QW line widths of the as-grown sample and nanopillars are 49.7 ± 0.77 meV (4.35 nm) and 60.1 ± 0.8 meV (5.27 nm), respectively. These values are only half that for results reported in similar structures in ref 19, which is 11.2 nm at room temperature. They are also comparable to the results obtained by a nonpolar m-plane $Al_xGa_{1-x}N/Al_yGa_{1-y}N$ multiple QWs, which are 5.13 nm (112 meV) at 9 K and 6.08 nm (132 meV) at room temperature.20 Increasing the temperature also reduces the signatures of the SLs and buffer layers; a superposition of the peaks from different layers can be observed in Figure 3b. At both low and high temperatures, the peaks of the SLs cannot be observed from the nanopillar sample; the PL emission suppression may be caused by surface damage introduced by the etching or surface states which can quench the SL emission preferentially.

Figure 4 depicts the excitation power dependence of the PL characteristics of the two samples measured at 5 and 300 K. The average input excitation power was increased from 30 μW to 2 mW measured before the μPL setup. The total transmission efficiency of the optical mirrors, dichroic glass, and UV objective is ∼20%, and the laser spot diameter on the sample is ∼2 μm. We can see that over a wide excitation power density range both samples exhibit an almost unchanged QW peak wavelength and fwhm (especially at low temperature), in contrast to typically reported blue-shifts and significant broadening effects.[17,18,21] With enhanced excitation power, the peak energy decreases slightly in wavelength by <6 meV at both low and high temperatures. There are several mechanisms responsible for the peak energy shifts, such as the red-shift due to the carrier induced bandgap renormalization (BGR) and dopants[11,22−25] and the blue-shift due to QCSE screening and band filling (also known as the Burstein−Moss shift).[22,26−29]

For nanopillars, thermal effects may also lead to a red-shift.[17,30] Although the competition principles of the above mechanisms are controversial, here we believe the strain in our QW is well relaxed due to the insertion of the SLs; therefore, the QCSE is greatly reduced, and the blue-shift that could be caused by QCSE screening is negligibly small. For the BGR, the energy shift for relaxed material is about $Eg = -Kn^{1/3}$ eV cm, where K is the bandgap coefficient (∼2.6 × 10−8 eV cm) and n is the carrier density.[31−33] The photogenerated carrier density can be estimated by $\Delta n = (A \times (1 - R) \times \alpha)/h\nu$, where A is the energy density of the pump laser, R is the intensity reflectance, α is the absorption coefficient of the sample, and $h\nu$ is the laser photon energy. From the literature, the reflection and absorption coefficients of $Al_{0.3}Ga_{0.7}N$ under the injection of a 266 nm laser are ∼20% and 16 × 104 cm^{-1}, respectively.[34,35] With the given power range and repetition rate stated above, the photogenerated carrier density ranges from 1 × 1017 to 6.8 × 1018 cm^{-3}. Hence, the bandgap could change from −12.2 to −49.3 meV. As a result of the counteraction between the band-filling effect and the BGR, the peak emission variation with excitation power is almost negligible, providing a very stable output wavelength. Figure 4 also illustrates that at 5 K the changes of the fwhm with excitation power are <3.5 meV (<0.3 nm) coming from the higher energy states filled by more excited carriers, showing a near-constant behavior.[27,36] Generally, the screening of QCSE with increasing excitation always comes along with a narrowing of the line width.[22,27] Here the lack of this behavior in the excitation power dependence of the fwhm proves one more time that the QCSE in the QW is effectively reduced. At 300 K, the broadening of the fwhm is <11.3 meV (<1 nm) for the as-grown sample and about 14.2 meV (1.25 nm) for the nanopillars, which is still relatively insensitive to excitation power. At 300 K, besides the band-filling effects, the interaction between the carriers and nonradiative recombination centers also contributes to this phenomenon.[33] In addition to the above effects, pillar-to-pillar inhomogeneous broadening also exists in nanopillars.[37]

To understand the exciton localization effects of the QW structure grown on SLs, the temperature dependence from 5 to 300 K of the PL spectra was measured with an excitation power of 100 μW. In general, the temperature-dependent behavior is attributed to the potential inhomogeneity and localized character of the carrier recombination.[38] The increasing temperature will induce a band gap shrinkage which is described by the Varshni equation[39,40]

$$E(T) = E_g(0K) - \frac{\alpha T^2}{T + \beta} - \sigma^2/k_B T$$

where E_g(0 K) is the transition energy of GaN QW at 0 K, α and β are the Varshni coefficients, σ indicates the degree of the localization effect, and kB is the Boltzmann constant. As Figure 5 depicts, the peak energies of both samples do not follow the expected Varshni equation (see dashed line in Figure 5). A best fit of α = 1.15 meV/K, β = 1050 K, E_g(0 K) = 3.84 eV ± 1.2 meV, and σ = 18 meV was obtained for the as-grown sample by excluding the data below 100 K and α = 0.89 meV/K, β = 1000 K, E_g(0 K) = 3.83 eV ± 0.7 meV, and σ = 10.5 meV for the nanopillars by excluding the data below 50 K. The two samples show an "S-shape" for the peak energy (red-shift, blueshift, and then red-shift) and a weak "W-shape" for the line width (increase, decrease, and then increase) with rising temperature. Similar phenomena were reported in refs 38 and 40−43. For 5 K < T < 50 K, the 10 meV red-shift and moderately wider line width can be interpreted as weakly localized carriers being thermally activated by the increasing temperature, having a greater opportunity to migrate to deeper localized states. As the temperature is further increased from 50 to ~140 K, a thermal equilibrium is achieved and the carriers occupy higher levels, which results in a blue-shift of ~10 meV. The increase of the fwhm up to 50 K is the crossover from nonthermalized to thermalized energy distribution of localized excitons. Between 50 and 140 K, the fwhm becomes slightly narrower and then wider because of the high mobility of the carriers even in deep localized states.[41] At temperatures above ~100 K (~50 K for nanopillars), higher energy states are increasingly occupied by photoexcited carriers. The peak energy behavior becomes consistent with Varshni's equation and decreases with increasing temperature. The carrier interactions with activated nonradiative recombination centers and phonons make the line width broader from 80 to 300 K. The relatively shallow localization depths of the two samples illustrate a reduced phase separation in the well because of the relaxed strain and also a relatively low inhomogeneity in both the well and SL layers. A fluctuating Al content in the barriers may also modify the energy bands. However, a fluctuation of about ±20%−60% of the Al molar fraction in the barriers is needed to account for the localization energies.[43] Therefore, the effect of Al content fluctuations can be ruled out in our samples.

To get more insight into the carrier recombination dynamics of the QW on the SLs, TR-μPL spectra were measured as a function of excitation power and temperature. Fitting of the lifetime data was performed using the modified Gaussian function as follows[44]

$$f(t) = f_0 + (f_{\mathrm{Gauss}} \otimes f_{\mathrm{exp}} \quad (2)$$

where f_{Gauss} is the instrument response function (IRF) of the PMT, which can be approximated with a Gaussian profile with a fwhm of ~130 ps. As seen in Figure 6a,b, the carrier recombination dynamics depend on the excitation power at low temperature. For the as-grown sample at 5 K, the decay time is 1.1 ± 0.02 ns at 10 μW excitation power and decreases to 0.6 ± 0.01 ns at 1.7 mW excitation power; for the nanopillars at 5 K, the decay time is 0.8 ± 0.0 2 ns at 10 μW excitation power and decreases to 0.47 ± 0.01 ns at 1.7 mW excitation power. The decay time decreases more strongly with higher excitation power up to ~400 μW and then becomes quite stable with stronger excitation power. Basically, the lifetime can be in a range from several picoseconds to several nanoseconds (or even longer), depending on several factors, such as the carrier recombination both in QW and localized states as well as the nonradiative recombination introduced by defects at higher temperature. At 5 K, the PL lifetime is dominated by the radiative recombination lifetime, containing both radiative free-exciton recombination and radiative recombination at localized states. The relatively longer lifetime of the samples may because of the Al-rich AlGaN localized structures exist in the QW due to the Al content fluctuations. When the excitation power begins to increase, the majority of carriers recombine at the localized states. The measured PL lifetime is mainly that of the localized carriers. As the excitation power is further increased, the localized states saturate and cannot trap more carriers; hence, the free-exciton lifetime dominates.[45] At 300 K, the decay time of the PL does not change much with intensity because the recombination process is already dominated by non-radiative recombination. At both 5 and 300 K the PL decay time of the nanopillars is shorter than that of the as-grown sample. That is because the etching process of the nanopillar sample produces more surface states which can act as traps for the carriers; the relaxation of the small remaining QCSE in the nanopillars has some contributions as well at low temperature.

Figure 7a shows the PL decay time of the two samples as a function of temperature. As can be seen from the traces, when the temperature increases, the decay time of the two samples initially increases slightly and then drops. At around 10 K, deeper localized states are thermally activated and capture carriers, making the lifetime longer. It is also the Temperature range in which the red-shift occurs as shown in Figure 5. When the temperature is increased to above 50 K, defects and other nonradiative recombination centers are activated. The carriers are captured by them before recombining at the localized states, which makes the PL decay time decreases quickly. It is the temperature range in which a blue-shift of the PL peak energy is observed in Figure 5. Above 100 K, the PL lifetime is relatively steady which is caused by the dominance of nonradiative recombination. The results of the temperature-dependent recombination dynamics are consistent with those for the peak energies discussed earlier in this paper. The PL decay time is generally faster in nanopillars than in as-grown samples because of surface trapping effects and further relaxed QCSE. Figure 7b shows Arrhenius plots of the temperature-dependent PL intensities of the two samples from 5 to 300 K. It can be observed that the PL intensity decreases with temperature as a result of the strong nonradiative recombination.

To confirm that the use of the SLs effectively relaxes the strain in the QW on top of them, Raman spectroscopy was conducted which provided important information about the strain state of the structures. GaN, InN, AlN, and their alloys in wurtzite structure belong to the C_{6v}^{4}space group, containing eight sets of phonon modes: $2E_2$ modes, $2E_1$ modes, $2A_1$ modes, and $2B_1$ modes.[46−48] The E_1 and A_1 modes are both Raman- and IR-active, B_1 modes are silent, and E_2(high) modes are only Raman-active. Generally, the E_2(high) mode is sensitive to strain in the structure; its peak shift and intensity change are used to accurately determine the strain state. With a 180° backscattering configuration, the Raman phonon modes of the two samples follow the selection rules as shown in Table 1,[49,50] where the *Z*-axis is along the crystallographic *c*-axis of sapphire.

The room-temperature μ-Raman spectra of the two samples are shown in Figure 8, measured in the $Z(XX)\bar{Z}$ backscattering and the nanopillars are 574.4 ± 0.15 and 573.7 ± 0.17 cm^{-1}, respectively. There are slight red-shifts of the two modes compared to that of the strain-free $Al_{0.3}Ga_{0.7}N$. It means that only moderate compressive strain exists in the QW. The GaN-like E_2(high) frequencies of the nanopillars are lower than that of the as-grown sample, indicating that the nanopillars exhibit further relaxed strain.

Conclusions

In this work, we have investigated the optical performance and the underlying physical mechanisms of a $GaN/Al_{0.3}Ga_{0.7}N$ single QW with graded Al content SLs layers systematically. The as-grown sample was grown with two groups of SLs strain relaxing layers on a c-plane sapphire and then fabricated into nanopillars for strain comparison. From TI-μPL and TR-μPL spectroscopy we find that the QW emissions of both samples are very sharp in UV region and nearly constant over a wide excitation power range from 30 μW to 2 mW with only a 6 meV slight red-shift. This effect is the interplay between the BGR and band filling as well as the reduced QCSE. The fwhm is also quite insensitive to excitation power, especially at low temperature. At 300 K, the moderately broadened fwhm with stronger excitation power can be attributed to the interactions with non-radiative recombination and the band filling. "S-shape" and "weak W-shape" temperature dependences of the QW peak energy and fwhms are the combination of the carrier scattering mechanisms and thermally dependent localization effects as well as nonradiative recombination. The excitation power and temperature dependences of the PL lifetime were also investigated. At 5 K, with increasing excitation power, extra photoexcited carriers shorten the carrier recombination lifetime because of the saturation of the localized states. The radiative lifetime of the nanopillars is 0.46 ns at 5 K. At 300 K, nonradiative recombination centers dominate and are insensitive with excitation power. Higher temperature leads to faster PL lifetimes, as the injected carriers escape much more easily from localized states and also interact non-radiatively. In addition, we studied the Raman spectra of the two samples, proving that the SLs effectively suppressed the strain. From all the experimental results presented above we find that the QW structures with SLs show several very desirable characteristics: very narrow and strong UV emission even at room temperature, nearly constant wavelength and very stable fwhm over a wide range of excitation power, and a relatively fast radiative recombination time. It is reasonable to conclude that by carefully designing the SLs layers, we can realize almost zero-strain effects which is generally observed in nonpolar structure, confine and accumulate carriers, suppress some nonradiative recombination, and have very stable optical performance, which are highly helpful for GaN-based UV optoelectronic devices.

Associated Content

The Supporting Information is available free of charge at https://pubs.acs.org/doi/10.1021/acsaelm.9b00813. Additional details of the cathodoluminescence measurement of nanopillars, the estimation of the carrier density generated by excitation laser, and the GaussMod fitting of the decay time and the instrument response function (PDF).

Author Information

Corresponding Authors
Jian Zhang − Microsystem and Terahertz Research Center (CAEP), Chengdu 610200, China; School of Electronics Science and Engineering, University of Electronic Science and Technology of China, Chengdu 610054, China; Email: jianzhang@uestc.edu.cn

Robert A. Taylor − Department of Physics, University of Oxford, Oxford OX1 3PU, United Kingdom; orcid.org/ 0000-0003-2578-9645; Email: robert.taylor@physics.ox.ac.uk

Authors
Mo Li − Microsystem and Terahertz Research Center (CAEP), Chengdu 610200, China; School of Electronics Science and Engineering, University of Electronic Science and Technology of China, Chengdu 610054, China; orcid.org/0000-0001-8413-2497

Feiliang Chen − Microsystem and Terahertz Research Center (CAEP), Chengdu 610200, China

Claudius Kocher − Department of Physics, University of Oxford, Oxford OX1 3PU, United Kingdom; orcid.org/0000-0002-7785-1968

Hui Zhang − Microsystem and Terahertz Research Center (CAEP), Chengdu 610200, China

Shuxiao Li − Microsystem and Terahertz Research Center (CAEP), Chengdu 610200, China

Feng Huang − Microsystem and Terahertz Research Center (CAEP), Chengdu 610200, China

Complete contact information is available at:
https://pubs.acs.org/10.1021/acsaelm.9b00813

Author Contributions
M.L. conducted all the experiments, analyzed all the data, and wrote the manuscript; F.C. fabricated the samples and helped with the data analyses; C.K. built the optical setup and helped with the experiments; H.Z. performed the SEM and TEM measurements; S.L. and F.H. helped with the device fabrication; R.A.T. and J.Z. designed and supervised all experiments and contributed to the discussions. All authors have given approval to the final version of the manuscript.

Notes
The authors declare no competing financial interest.

Acknowledgments

The authors gratefully acknowledge Prof. Weikun Ge (Tsinghua University), Dr. Qian Li (MTRC), and Dr. Jian Zhang (Xiamen University) for useful discussions. This work is supported by the Science Challenge Project (Grant TZ2016003-2), the National Natural Science Foundation of China (NSFC) (Grants 61875178 and 61704062), and the China Scholarship Council Project (Grant 201804890005).

References

(1) Kneissl, M. A Brief Review of III-nitride UV Emitter Technologies and Their Applications. In III-Nitride Ultraviolet Emitters; Kneissl, M., Rass, J., Eds.; Springer Series in Materials Science; Springer: Cham, 2016; Vol. 227.
(2) Li, D.; Jiang, K.; Sun, X.; Guo, C. AlGaN Photonics: Recent Advances in Materials and Ultraviolet Devices. Adv. Opt. Photonics 2018, 10 (1), 43−110.
(3) Kneissl, M.; Kolbe, T.; Chua, C.; Kueller, V.; Lobo, N.; Stellmach, J.; Knauer, A.; Rodriguez, H.; Einfeldt, S.; Yang, Z.; Johnson, N. M.; Weyers, M. Advances in Group III-Nitride-Based Deep UV Light-Emitting Diode Technology. Semicond. Sci. Technol. 2011, 26, 014036.

(4) Drost, R. J.; Sadler, B. M. Survey of Ultraviolet Non-Line-of-Sight Communications. Semicond. Sci. Technol. 2014, 29, 084006.
(5) Leroux, M.; Grandjean, N.; Laügt, M.; Massies, J.; Gil, B.; Lefebvre, P.; Bigenwald, P. Quantum Confined Stark Effect Due to Built in Internal Polarization Fields in (Al, Ga)N/GaN Quantum Wells. Phys. Rev. B: Condens. Matter Mater. Phys. 1998, 58 (20), 13371.
(6) Miller, D.; Chemla, D.; Damen, T.; Gossard, A.; Wiegmann, W.; Wood, T.; Burrus, C. Band-Edge Electroabsorption in Quantum Well Structures: The Quantum-Confined Stark Effect. Phys. Rev. Lett. 1984, 53 (22), 2173−2176.
(7) Rashidi, A.; Monavarian, M.; Aragon, A.; Okur, S.; Nami, M.; Rishinaramangalam, A.; Mishkat-Ul-Masabih, S.; Feezell, D. High-Speed Nonpolar InGaN/GaN LEDs for Visible-Light Communication. IEEE Photonics Technol. Lett. 2017, 29 (4), 381−384.
(8) Jiu, L.; Gong, Y.; Wang, T. Overgrowth and Strain Investigation of (11−20) Non-Polar GaN on Patterned Templates on Sapphire. Sci. Rep. 2018, 8, 41598.
(9) Mu, Q.; Xu, M.; Wang, X.; Wang, Q.; Lv, Y.; Feng, Z.; Xu, X.; Ji, Z. Influence of The InGaN/GaN Quasi-Superlattice Underlying Layer on Photoluminescence in InGaN/GaN Multiple Quantum Wells. Phys. E 2016, 76, 1−5.
(10) Ley, R.; Chan, L.; Shapturenka, P.; Wong, M.; DenBaars, S.; Gordon, M. Strain Relaxation of InGaN/GaN Multi-Quantum Well Light Emitters Via Nanopatterning. Opt. Express 2019, 27 (21), 30081−30089.
(11) Tsai, C.-L. Effects of Underlying InGaN/GaN Superlattice Structrues on the Structural and Optical Properties of InGaN LEDs. J. Lumin. 2016, 174, 36−41.
(12) Sugahara, T.; Lee, J. S.; Ohtsuka, K. Role of AlN/GaN Multilayer in Crack-Free Layer Growth on 5”φ Si (111) Substrate. Jpn. J. Appl. Phys. 2004, 43 (12B), 1595−1597.
(13) Einfeldt, S.; Heinke, H.; Kirchner, V.; Hommel, D. Strain Relaxation in AlGaN/GaN Superlattices Grown on GaN. J. Appl. Phys. 2001, 89 (4), 2160−2167.
(14) Lin, P.-J.; Huang, S.-Y.; Wang, W.-K.; Chen, C.-L.; Chung, B.-C.; Wuu, D.-S. Controlling the Stress of Growing GaN on 150-mm Si(111) in an AlN/GaN Strained Layer Superlattice. Appl. Surf. Sci. 2016, 362, 434−440.
(15) Huang, C. C.; Xu, F. J.; Song, J.; Xu, Z. Y.; Wang, J. M.; Zhu, R.; Chen, G.; Wang, X. Q.; Yang, Z. J.; Shen, B.; Chen, X. S.; Lu, W. Different Strain Relief Behaviors in Al0.35Ga0.65N/GaN Multiple Quantum Wells on GaN/Sapphire Templates with AlN/GaN Superlattices and Low-Temperature AlN Interlayers. J. Appl. Phys. 2012, 111 (1), 016105.
(16) Matsumoto, T.; Khan, M. A.; Maeda, N.; Fujikawa, S.; Kamata, N.; Hirayama, H. Milliwatt Power UV-A LEDs Developed by Using N-AlGaN Superlattice Buffer Layers Grown on AlN Templates. J. Phys. D: Appl. Phys. 2019, 52, 115102.
(17) Li, Q.; Westlake, K. R.; Crawford, M. H.; Lee, S. R.; Koleske, D.D.; Figiel, J. J.; Cross, K. C.; Fathololoumi, S.; Mi, Z.; Wang, G. T. Optical Performance of Top-Down Fabricated InGaN/GaN Nanorod Light Emitting Diode Arrays. Opt. Express 2011, 19 (25), 25528−25534.
(18) Dong, P.; Yan, J.; Zhang, Y.; Wang, J.; Geng, C.; Zheng, H.; Wei, X.; Yan, Q.; Li, J. Optical Properties of Nanopillar AlGaN/GaN MQW for Ultraviolet Light-Emitting Diodes. Opt. Express 2014, 22 (S2), 320−327.
(19) Janjua, B.; Sun, H.; Zhao, C.; Anjum, D. H.; Priante, D.; Alhamoud, A. A.; Wu, F.; Li, X.; Albadri, A. M.; Alyamani, A. Y.; El- Desouki, M. M.; Ng, T. K.; Ooi, B. S. Droop-Free AlxGa1-xN/AlyGa1-yN Quantum-Disk-in-Nanowires Ultraviolet LED Emitting at 337 nm on Metal/Silicon Substrates. Opt. Express 2017, 25 (2), 1381−1390.
(20) Banal, R. G.; Taniyasu, Y.; Yamamoto, H. Deep-Ultraviolet Light Emission Properties of Nonpolar M-Plane AlGaN Quantum Wells. Appl. Phys. Lett. 2014, 105 (5), 053104.

(21) Kawakami, Y.; Kaneta, A.; Su, L.; Zhu, Y.; Okamoto, K.; Funato, M.; Kikuchi, A.; Kishino, K. Optical Properties of InGaN/GaN Nanopillars Fabricated by Postgrowth Chemically Assisted Ion Beam Etching. J. Appl. Phys. 2010, 107, 023522.
(22) Slimane, A. B.; Najar, A.; Elafandy, R.; San-Román-Alerigi, D.P.; Anjum, D.; Ng, T. K.; Ooi, B. S. On the Phenomenon of Large Photoluminescence Red-Shift in GaN Nanoparticles. Nanoscale Res. Lett. 2013, 8, 342.
(23) Aleksandrov, I.; Zhuravlev, K. Photoluminescence of GaN/AlN Quantum Dots at High Excitation Powers. Phys. Status Solidi C 2010, 7, 2230−2232.
(24) Wang, Y. J.; Xu, S. J.; Li, Q.; Zhao, D. G.; Yang, H. Band Gap Renormalization and Carrier Localization Effects in InGaN/GaN Quantum-Wells Light Emitting Diodes with Si Doped Barriers. Appl. Phys. Lett. 2006, 88, 041903.
(25) Reshchikov, M. A.; Morkoç, H. Luminescence Properties of Defects in GaN. J. Appl. Phys. 2005, 97, 061301.
(26) Kazlauskas, K.; Tamulaitis, G.; Mickevičius, J.; Kuokštis, E.; Žukauskas, A.; Cheng, Y.-C.; Wang, H.-C.; Huang, C.-F.; Yang, C. C. Excitation Power Dynamics of Photoluminescence in InGaN/GaN Quantum Wells with Enhanced Carrier Localization. J. Appl. Phys. 2005, 97, 013525.
(27) Wang, H.; Ji, Z.; Qu, S.; Wang, G.; Jiang, Y.; Liu, B.; Xu, X.; Mino, H. Influence of Excitation Power and Temperature on Photoluminescence in InGaN/GaN Multiple Quantum Wells. Opt. Express 2012, 20, 3932−3940.
(28) Chichibu, S.; Azuhata, T.; Sota, T.; Nakamura, S. Spontaneous Emission of Localized Excitons in InGaN Single and Multi-quantum Well Structures. Appl. Phys. Lett. 1996, 69, 4188.
(29) Eliseev, P. G.; Perlin, P.; Lee, J.; Osiński, M. 'Blue' Temperature-Induced Shift and Band-Tail Emission in InGaNBased Light Sources. Appl. Phys. Lett. 1997, 71, 569.
(30) Chin, A. H.; Ahn, T. S.; Li, H.; Vaddiraju, S.; Bardeen, C. J.; Ning, C.-Z.; Sunkara, M. K. Photoluminescence of GaN Nanowires of Different Crystallographic Orientation. Nano Lett. 2007, 7 (3), 626−631.
(31) Lee, I.-H.; Lee, J. J.; Kung, P.; Sanchez, F. J.; Razeghi, M. Band-Gap Narrowing and Potential Fluctuations in Si-doped GaN. Appl. Phys. Lett. 1999, 74 (1), 102−104.
(32) Schenk, H. P. D.; Borenstain, S. I.; Berezin, A.; Schön, A.; Cheifetz, E.; Khatsevich, S.; Rich, D. H. Band Gap Narrowing and Radiative Efficiency of Silicon Doped GaN. J. Appl. Phys. 2008, 103, 103502.
(33) Yoshikawa, M.; Kunzer, M.; Wagner, J.; Obloh, H.; Schlotter, P.; Schmidt, R.; Herres, N.; Kaufmann, U. Band-gap Renormalization and Band Filling in Si-doped GaN Films Studied by Photoluminescence Spectroscopy. J. Appl. Phys. 1999, 86 (8), 4400−4402.
(34) Muth, J. F.; Brown, J. D.; Johnson, M. A. L.; Yu, Z.; Kolbas, R. M.; Cook, J. W.; Schetzina, J. F. Absorption Coefficient and Refractive Index of GaN, AlN and AlGaN Alloys. MRS Internet J. Nitride Semicond. Res. 1999, 4, 502−507.
(35) Akinlami, J. O.; Olateju, I. O. Reflection Coefficient and Optical Conductivity of Gallium Nitride GaN. Fiz. Napivprovidn., Kvantova Optoelektron. 2012, 15, 281−284.
(36) Sun, H.; Ji, Z.; Wang, H.; Xiao, H.; Qu, S.; Xu, X.; Jin, A.; Yang, H. Transfer and Recombination Mechanism of Carriers in Phase-Separated InGaN Quantum Wells. J. Appl. Phys. 2013, 114, 093508.
(37) Rigutti, L.; Tchernycheva, M.; De Luna Bugallo, A.; Jacopin, G.; Julien, F. H.; Zagonel, L. F.; March, K.; Stephan, O.; Kociak, M.; Songmuang, R. Ultraviolet Photodetector Based on GaN/AlN Quantum Disks in a Single Nanowire. Nano Lett. 2010, 10 (8), 2939−2943.
(38) Rosales, D.; Gil, B.; Bretagnon, T.; Guizal, B.; Zhang, F.; Okur, S.; Monavarian, M.; Izyumskaya, N.; Avrutin, V.; Ozgur, U.; Morkoc, H.; Leach, J. H. Excitonic Recombination Dynamics in Non-Polar GaN/AlGaN Quantum Wells. J. Appl. Phys. 2014, 115 (7), 073510.

(39) Varshni, Y. P. Temperature Dependence of the Energy Gap in Semiconductors. Physica (Amsterdam) 1967, 34, 149−154.
(40) Bai, J.; Wang, T.; Sakai, S. Influence of the Quantum-Well Thickness on the Radiative Recombination of InGaN/GaN Quantum Well Structures. J. Appl. Phys. 2000, 88, 4729.
(41) Cho, Y.-H.; Gainer, G. H.; Fischer, A. J.; Song, J. J.; Keller, S.; Mishra, U. K.; DenBaars, S. P. S-shaped" Temperature-Dependent Emission Shift and Carrier Dynamics in InGaN/GaN Multiple Quantum Wells. Appl. Phys. Lett. 1998, 73 (10), 1370−1372.
(42) Li, J.; Li, C.; Xu, M.; Ji, Z.; Shi, K.; Xu, X.; Li, H.; Xu, X. "Wshaped" Injection Current Dependence of Electroluminescence Linewidth in Green InGaN/GaN-Based LED Grown on Silicon Substrate. Opt. Express 2017, 25, 871−879.
(43) Wu, F.; Zhang, J.; Wang, S.; Long, H.; Dai, J.; Feng, Z.; Gong, Z.; Chen, C. Quantum Confinement Dependence of Exciton Localization in a-Plane GaN/AlGaN Multiquantum Wells Investigated by Temperature Dependent Photoluminescence. Opt. Mater. Express 2015, 5, 2608−2615.
(44) Wang, T.; Puchtler, T. J.; Zhu, T.; Jarman, J. C.; Nuttall, L. P.; Oliver, R. A.; Taylor, R. A. Polarisation-Controlled Single Photon Emission at High Temperature from InGaN Quantum Dots. Nanoscale 2017, 9, 9421−9427.
(45) Lefebvre, P.; Allegre, J.; Gil, B.; Kavokine, A.; Mathieu, H.; et al. Recombination Dynamics of Free and Localized Excitons in GaN/Ga0.93Al0.07N Quantum Wells. Phys. Rev. B: Condens. Matter Mater. Phys. 1998, 57 (16), 9447−9450.
(46) Lee, I.-H.; Choi, I.-H.; Lee, C.-R.; Shin, E.-J.; Kim, D.; Noh, S. K.; Son, S.-J.; Lim, K. Y.; Lee, H. J. Stress Relaxation in Si-doped GaN Studied by Raman Spectroscopy. J. Appl. Phys. 1998, 83 (11), 5787−5791.
(47) Tripathy, S.; Chua, S. J.; Chen, P.; Miao, Z. L. Micro-Raman Investigation of Strain in GaN and AlxGa1-xN/GaN Heterostructures Grown on Si(111). J. Appl. Phys. 2002, 92 (7), 3503−3510.
(48) Puech, P.; Demangeot, F.; Frandon, J.; Pinquier, C.; Kuball, M.; Domnich, V.; Gogotsi, Y. GaN Nanoindentation: A Micro-Raman Spectroscopy Study of Local Strain Fields. J. Appl. Phys. 2004, 96 (5), 2853−2856.
(49) Kuball, M. Raman Spectroscopy of GaN, AlGaN and AlN for Process and Growth Monitoring/Control. Surf. Interface Anal. 2001, 31, 987−999.
(50) Irmer, G.; Roder, C.; Himcinschi, C.; Kortus, J. Raman Tensor Elements and Faust-Henry Coefficients of Wurtzite-Type α-GaN: How to Overcome the Dilemma of the Sign of Faust-Henry Coefficients in α-GaN? J. Appl. Phys. 2014, 116, 245702.
(51) Davydov, V. Yu.; Goncharuk, I. N.; Smirnov, A. N.; Nikolaev, A. E.; Lundin, W. V.; Usikov, A. S.; Klochikhin, A. A.; Aderhold, J.; Graul, J.; Semchinova, O.; Harima, H. Composition Dependence of Optical Energies and Raman Line Broadening in Hexagonal AlxGa1-xN Alloys. Phys. Rev. B: Condens. Matter Mater. Phys. 2002, 65, 125203.
(52) Ni, Y.; He, Z.; Yang, F.; Zhou, D.; Yao, Y.; Zhou, G.; Shen, Z.; Zhong, J.; Zhen, Y.; Wu, Z.; Zhang, B.; Liu, Y. Effect of AlN/GaN Superlattice Buffer on the Strain State in GaN-on-Si(111) System. Jpn. J. Appl. Phys. 2015, 54, 015505.

Figures & Tables

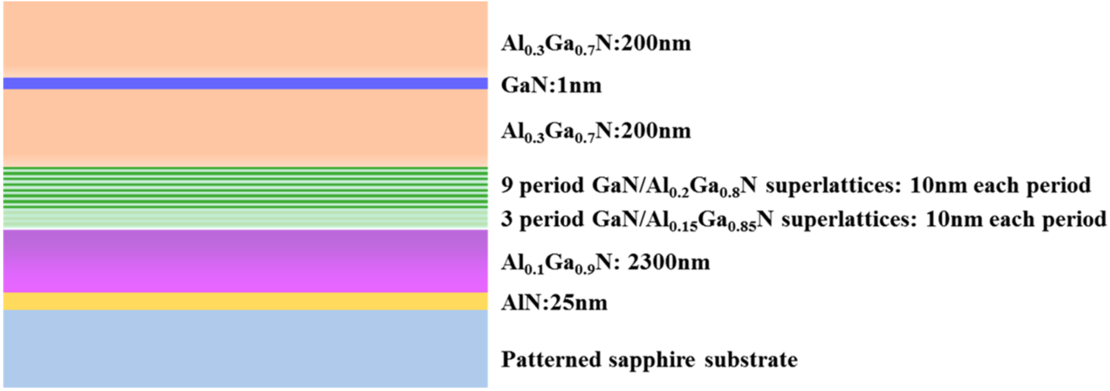

Figure 1. Schematic structure of a GaN/$Al_{0.3}Ga_{0.7}N$ single QW grown on SLs layers and *c*-plane sapphire.

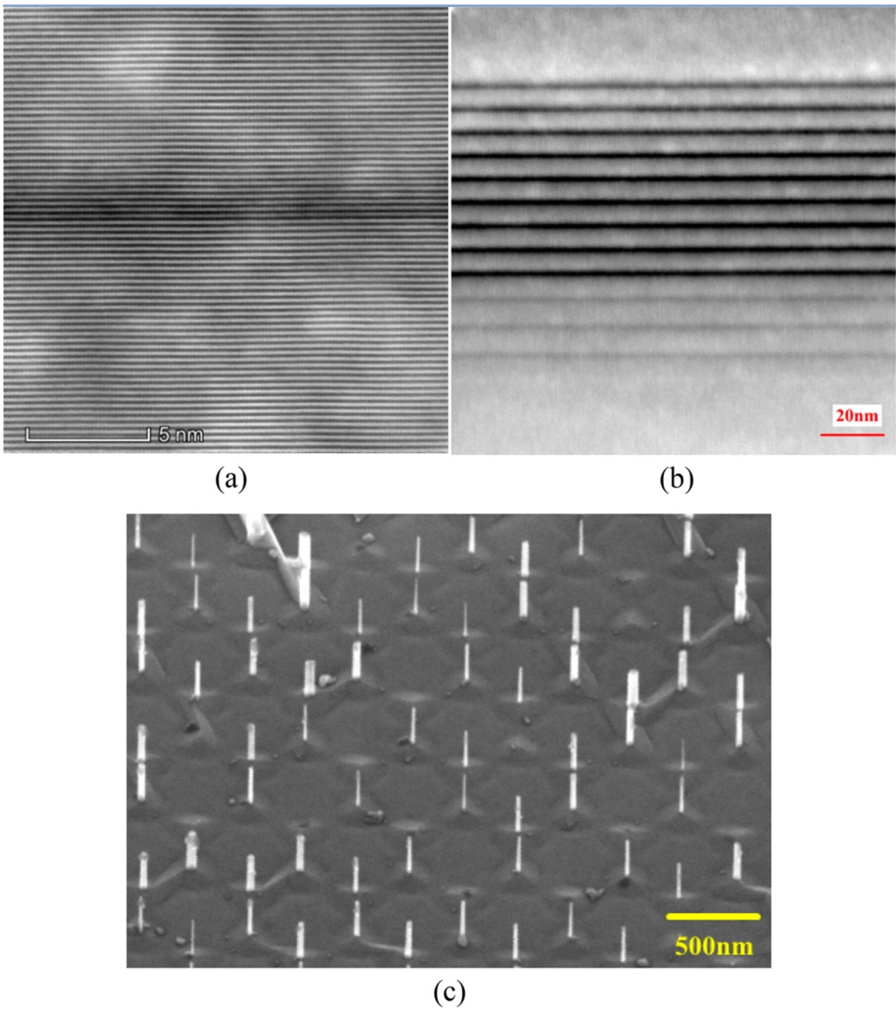

Figure 2. Side-view TEM images of (a) the single QW and (b) the two groups of SLs. (c) 45° tilted cross-sectional image of the nanopillar sample.

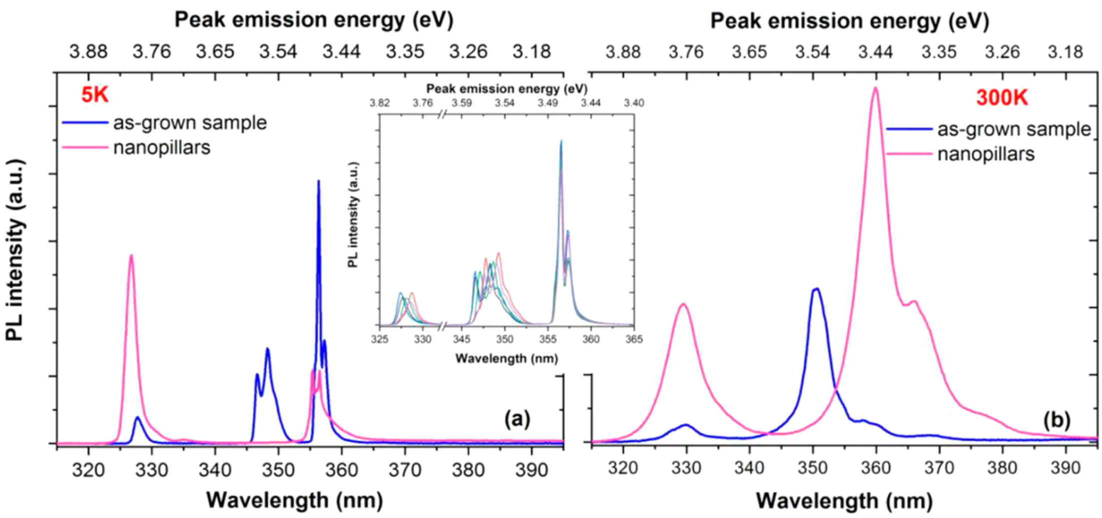

Figure 3. Time-integrated PL spectra of the as-grown sample and the dependent PL spectra of the as-grown sample at 5 K.

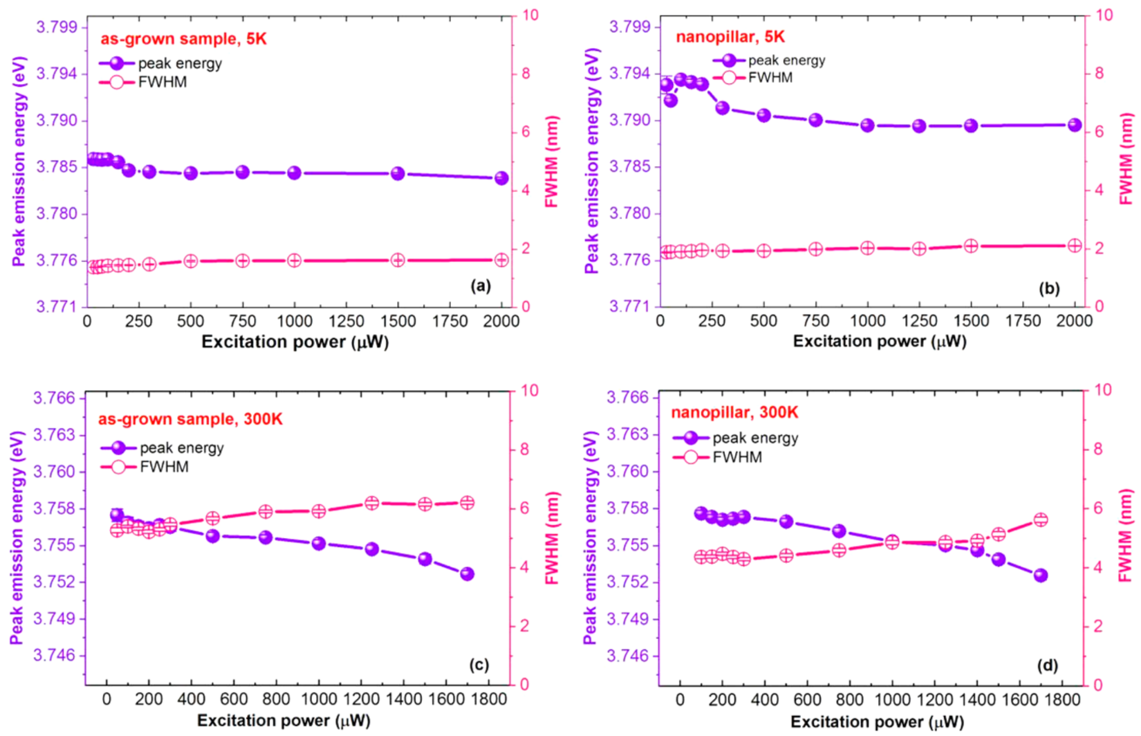

Figure 4. Excitation power dependence of the PL peak energy and the fwhm of (a) the as-grown sample at 5 K, (b) the nanopillar sample at 5 K, (c) the as-grown sample at 300 K, and (d) the nanopillar sample at 300 K.

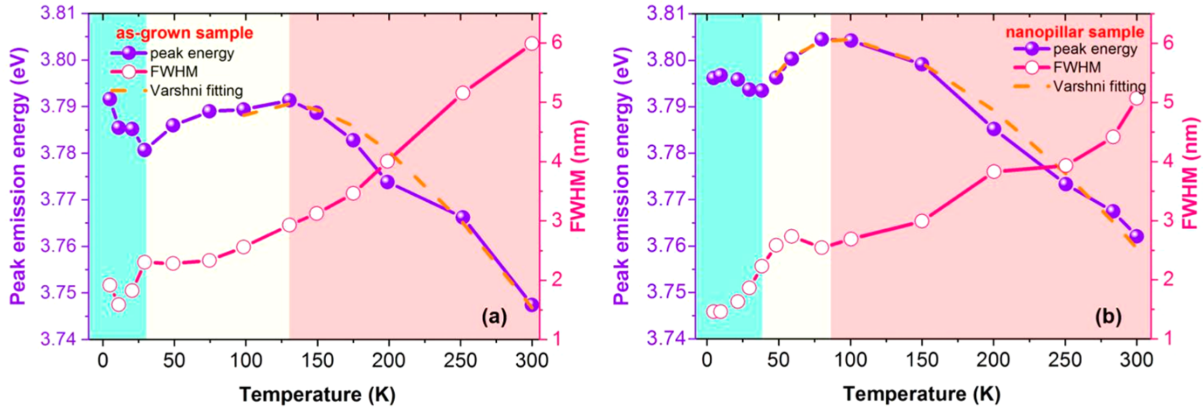

Figure 5. Temperature-dependent TI-μPL peak energy and fwhm of (a) the as-grown sample and (b) the nanopillar sample with an excitation power of 100 μW.

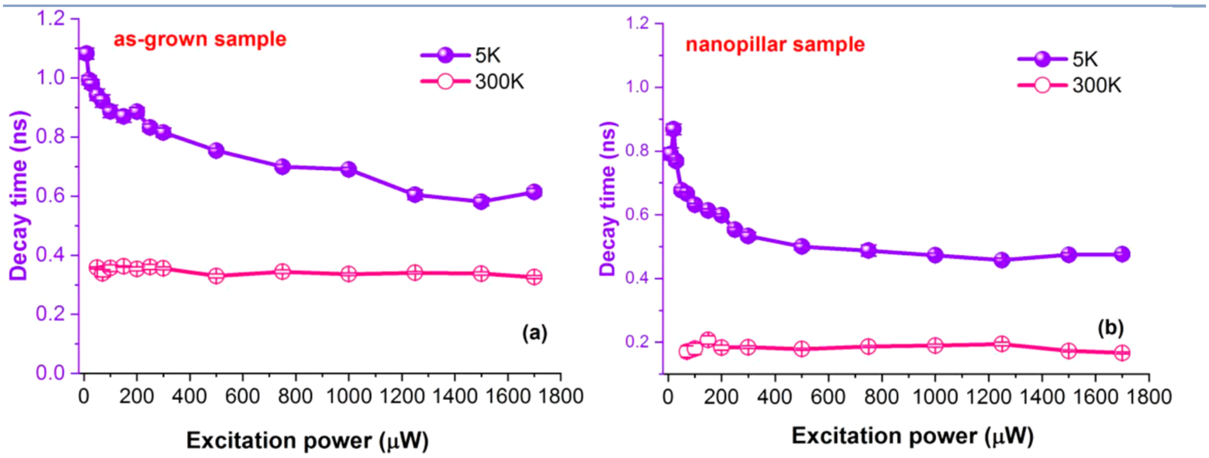

Figure 6. PL lifetime of (a) as-grown sample and (b) nanopillars versus excitation power at 5 and 300 K.

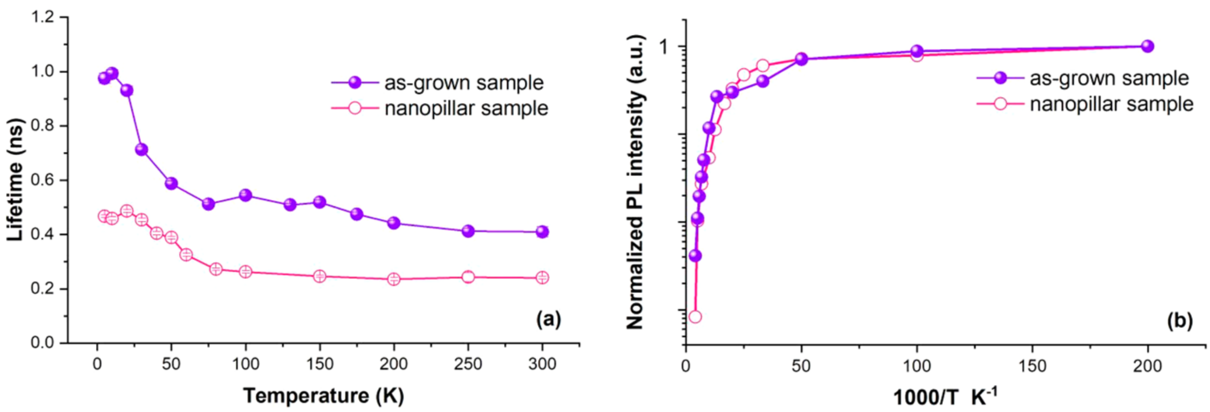

Figure 7. With an excitation power of 100 μW: (a) temperature dependence of the PL lifetime of the two samples; (b) Arrhenius plot of the PL intensities of the two samples as a function of temperature.

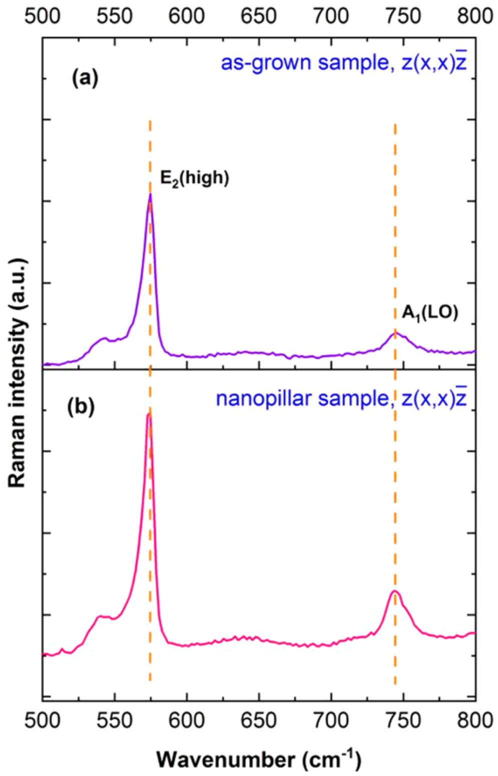

Figure 8. Micro-Raman spectra at room temperature of (a) the as- grown sample and (b) the nanopillar sample.

Table 1. Selection Rules of the Raman Modes of GaN, InN, AlN, and their Alloys

sample orientation	scattering configuration	allowed modes
(0001)	$Z(XX)\,\overline{Z}$	A_1 (LO), E_2 (high)
	$Z(XY)\,\overline{Z}$	E_2 (high)